



**HAL**  
open science

## Light Simulation with Participating Media

Romain Vavassori

► **To cite this version:**

| Romain Vavassori. Light Simulation with Participating Media. Graphics [cs.GR]. 2013. hal-00836663

**HAL Id: hal-00836663**

**<https://inria.hal.science/hal-00836663>**

Submitted on 21 Jun 2013

**HAL** is a multi-disciplinary open access archive for the deposit and dissemination of scientific research documents, whether they are published or not. The documents may come from teaching and research institutions in France or abroad, or from public or private research centers.

L'archive ouverte pluridisciplinaire **HAL**, est destinée au dépôt et à la diffusion de documents scientifiques de niveau recherche, publiés ou non, émanant des établissements d'enseignement et de recherche français ou étrangers, des laboratoires publics ou privés.



Master of Science in Informatics at Grenoble  
Master Mathématiques Informatique - spécialité Informatique  
option Graphics, Vision and Robotics

# Light Simulation with Participating Media

**Romain VAVASSORI**

June 20th, 2013

Research project performed at INRIA Rhône-Alpes

Under the supervision of:

Nicolas HOLZSCHUCH, INRIA

Defended before a jury composed of:

Prof. Remi RONFARD

Prof. James CROWLEY

Prof. Marie-Christine FAUVET

Prof. Lionel REVERET



## **Abstract**

In this project we address the problem of light scattering in participating materials. We create a complete simulation of this phenomenon in a more general case than previous work. We analyse the directional part of light, in order to install a clear basis for future work. We derive two models from this analysis: the spherical Gaussians approximation and the double exponential approximation. These models are placed in the scope of the planned development of an improved method for scattering. We also code a custom ray tracer to have a complete pipeline of rendering and to understand the underneath concepts. The validation of our simulation is done by comparing the results of d'Eon [2].

## **Résumé**

Dans ce projet, nous abordons le problème de la diffusion de la lumière dans des matériaux participant. Nous créons une simulation complète de ce phénomène dans un cas plus général que les travaux précédents. Nous analysons la partie directionnelle de la lumière, dans le but d'installer une base claire à de futurs travaux. Nous tirons deux modèles de cette analyse : l'approximation de gaussiennes sphériques et l'approximation de double exponentielle. Ces modèles sont placés dans le cadre de l'élaboration prévue d'une méthode amélioré pour la diffusion. Nous codons également un lanceur de rayons dans le but d'avoir un pipeline complet de rendu et de comprendre les concepts sous-jacents. La validation de notre simulation est effectuée en comparant les résultats de d'Eon [2].



# Contents

<b>Abstract</b>	<b>i</b>
<b>Résumé</b>	<b>i</b>
<b>1 Introduction</b>	<b>1</b>
<b>2 Working Environment</b>	<b>3</b>
<b>3 State of the Art</b>	<b>5</b>
3.1 Theory . . . . .	5
3.2 Related Work . . . . .	8
<b>4 Simulation and Analysis of Scattering Materials</b>	<b>13</b>
4.1 Study of the Behavior of Diffusion Approximation . . . . .	13
4.2 Finding a Better Description . . . . .	15
4.3 Ray Tracer . . . . .	21
4.4 Validation . . . . .	22
4.5 Future Work . . . . .	24
<b>5 Personal Experience</b>	<b>27</b>
<b>6 Conclusion</b>	<b>29</b>
<b>Bibliography</b>	<b>31</b>



## Introduction

Some materials exhibit scattering properties: light enters them, is scattered inside and leaves in a different place. These materials are omnipresent in our environment. Most of the liquids are in this case: milk, orange juice or coffee for instance, as well as other commonly used materials: skin, marble. The behavior of these materials is extremely challenging for illumination simulations.

This is an important problem because in these days, realistic rendering is a more and more appreciated domain. It tends to be very frequently used in modern video games as in *Battlefield 3* or *Uncharted 2* for instance, from which a major part of their promotion is based on their excellent graphics. Moreover the movie industry is also greatly interested in the realistic rendering, and in particular the field of special effects. These effects require to be as seamless as possible with reality and thus need the best physically accurate rendering. Recent action movies as *Iron Man*, *X-Men*, use a great amount of special effects. The animated movies are also a great domain for the research in computer graphics with movies like *Toy Story* or *Wall-E* for instance, which are completely produced by the mean of algorithms directly taken from computer graphics.

Light diffusion in scattering materials is not often used currently because of the complexity of this phenomenon and the relative subtlety of its effects in rendered images. However, as details makes the difference, realistic rendering can be greatly improved by the integration of methods simulating this type of scattering.

Current existing methods for participating media are either highly time consuming or coarse



*Battlefield 3*



*CryEngine*

Figure 1.1: *Realistic rendering is widely used in modern video games and cinema.*

approximations. The time consuming methods, such as path tracing are also the most precise because they simulate the complete behavior of light in scattering materials. The fast methods as the diffusion approximation are very coarse because they use a lot of restrictive hypothesis to solve the complex equations that are underneath the problem of scattering.

In this context we analyse the behavior of light in participating materials with a simulation of the scattering. From this analysis, we make two simplified models as the beginning of solving the problem of scattering. We also make a full ray tracer to have a complete pipeline of picture rendering.

## Working Environment

This research project takes place in INRIA research center (*Institut National de Recherche en Informatique et en Automatique*). INRIA is a research institute whose purpose is to cover the whole fields of applied mathematics and computer science. The teams of this institute regroup 1800 researchers as well as 1600 researchers from other organizations, and the budget of INRIA is about 233 million euros in 2013, among all research centers.

From an historical point of view, INRIA was found in 1967 with the initial objective of being at the cutting edge of the technology and educating the country in the field the computer science. Since these days, the laboratory has grown up to finally have research centers established in 8 different cities. For 20 years, INRIA has helped the creation of 80 company, registered patents and increased international collaborations.

This research project is performed in MAVERICK team (*Models and Algorithms for Visualization and Rendering*), at INRIA Grenoble (Monbonnot research center). MAVERICK is also a member of LJK research laboratory. This team is composed of about 20 people who work in the field of image synthesis.

MAVERICK team place itself at the end of the image production pipeline, when the pictures are generated and displayed. The inputs can vary widely as datasets, video flows, pictures and photographs or animated geometry from a virtual world, for instance. The outputs produced are pictures and videos.

These produced pictures will be viewed by humans, and this fact is considered as an important part of the research strategy of the team. It provides the benchmarks for evaluating the results: the pictures and animations produced must be able to convey the message to the viewer. The actual message depends on the specific application: data visualization, exploring virtual worlds, designing paintings, drawings and so on. All these applications share common research problems like ensuring that the important features are perceived, avoiding cluttering or aliasing, efficient internal data representation, for instance.

The aim of the team is producing representations and algorithms for efficient and high-quality computer generation of pictures and animations through several Research problems:

- Computer Visualization: representation of large dataset in an understandable way.
- Expressive Rendering: creation of artistic representations of virtual worlds.
- Illumination Simulation: modelling the interaction of light with objects.
- Complex Scenes: rendering and modelling highly complex scenes.

These research problems are addressed through three interconnected approaches which are: working on the impact of pictures with perceptual studies, developing representations for data and developing new methods for predicting the properties of a picture.

This master project falls within the scope of illumination Research problem with the aim of increasing the realism of produced pictures by improving existing methods in the field of subsurface light scattering.

## State of the Art

We will explain general theory underlying light behavior. The theory will describe what happen when light hits a material interface and how light interacts inside these materials. We will then describe the already existing techniques in the field of subsurface scattering.

### 3.1 Theory

In the following, we make some hypothesis concerning the light. We place ourselves in the case of geometrical optics, which describes light as rays travelling linearly through space, instead of waves. This is an excellent approximation in the case of the scale of the experiment being far larger than the wavelength of light, as in our case. The effects of light interference and diffraction are neglected with this abstraction because of their wave-like nature. Intensity of light, called radiance, is the quantity of radiation that passes through a surface within a certain solid angle. The unit of this quantity is  $[W m^{-2} sr^{-1}]$ .

When rays of light hit the surface of an object they are reflected according to a certain behavior. This reflection will depend on the geometry of the surface at a microscopic level as shown on Figure 3.1. Properties like diffuse and specular reflectance as well as roughness will depend on the regularity of the surface.

The statistical behavior of the surface at macroscopic level derives in the well known model of bidirectional reflectance distribution function (BRDF). BRDF is a 4D function  $f(\vec{\omega}_i, \vec{\omega}_o)$   $[sr^{-1}]$  of incoming light direction  $\vec{\omega}_i \in \mathbb{S}^2$  and outgoing light direction  $\vec{\omega}_o \in \mathbb{S}^2$ . This function describes the amount of light reflected by the surface of the material depending on the incoming and outgoing directions. The notion of diffuse reflectance and specular reflectance are generally used together to approximate the total reflecting behavior of a surface. The diffuse reflectance

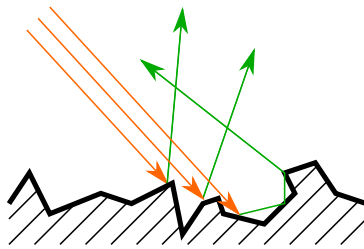


Figure 3.1: *Effect of a surface on the reflected light, at microscopic level.*

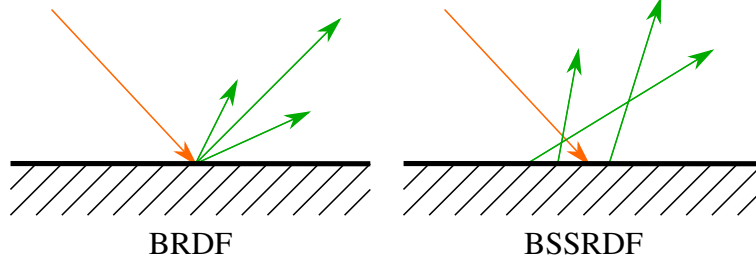


Figure 3.2: *BRDF and BSSRDF models for material reflection (macroscopic level).*

describes the amount of light that will be reflected equally in all directions, not depending of the incoming light direction. The specular reflectance describes the amount of light reflected in the direction symmetrically of the incoming light with respect to the surface plane normal. For instance mirrors are totally specular. Lambert, Gouraud and Phong are models of BRDF.

In our case we are interested in the interaction of light inside the material. BRDF is not able to describe this behavior and we thus need to use the bidirectional scattering surface reflectance distribution function (BSSRDF) [9]. BSSRDF is a generalization of BRDF as a 8D function  $S(x_i, \vec{\omega}_i, x_o, \vec{\omega}_o)$  [ $sr^{-1}$ ]. It adds two positional parameters  $x_i$  and  $x_o$  to the original BRDF function to account for light emitted at different position than from the position where incoming light strikes (see Figure 3.2). This generalization allows us to add to the model the interaction of light which enters the material at one position, scatters inside and exits the material at another position. Thus to know the outgoing radiance  $L_o$  at a point  $x_o$  we need to integrate BSSRDF over the surface  $A$  and all the directions of incoming light  $L_i$ :

$$L_o(x_o, \vec{\omega}_o) = \int_A \int_{2\pi} S(x_i, \vec{\omega}_i, x_o, \vec{\omega}_o) L_i(x_i, \vec{\omega}_i) (\vec{n} \cdot \vec{\omega}_i) d\omega_i dA(x_i)$$

**Subsurface light scattering and BSSRDF:** Scattering materials are composed of particles on which light will bounce. These particles create different effects on light. Light can be absorbed by the particle or scattered in another direction. The outgoing light is the sum of all paths that light has followed inside the material considering these several interactions before exiting at the surface. The phenomenon of refraction of light has also to be taken into account at the interface of the material. All these interactions are summarized in Figure 3.3.

At macroscopic level, these effects are described statistically. We introduce several quantities. First, the absorption coefficient  $\sigma_a$  [ $m^{-1}$ ] is the inverse of the average length after which the light will be absorbed by the material. The scattering coefficient  $\sigma_s$  [ $m^{-1}$ ], just as  $\sigma_a$ , is the inverse of the average length after which the light will be scattered. Finally the extinction coefficient is  $\sigma_t = \sigma_a + \sigma_s$  [ $m^{-1}$ ]. From  $\sigma_t$  results the mean free path (mfp) which is  $\frac{1}{\sigma_t}$  [ $m$ ] and represents the average length during which rays of light do not encounter obstacles. The albedo  $\alpha$  is the proportion of light that is reemitted relatively to the incoming light:  $\alpha = \frac{\sigma_s}{\sigma_a + \sigma_s}$ . An albedo of 1 means that all light is reflected while an albedo of 0 means that all light is absorbed by the material.

Finally, the phase function  $p(\vec{\omega}, \vec{\omega}')$  [ $sr^{-1}$ ] determines the statistical proportion of light emitted in a given direction  $\vec{\omega}'$  from the incoming direction of light  $\vec{\omega}$  when a scattering event occur (see Figure 3.4).

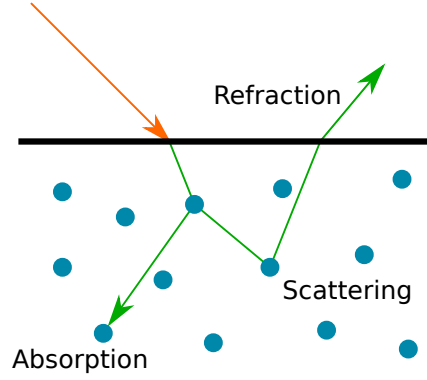


Figure 3.3: The effects of light interaction with particles inside the material.

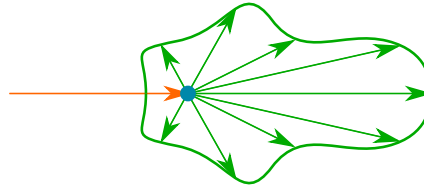


Figure 3.4: The amount of light in each direction after a scattering event is distributed according to the value of the phase function.

The propagation of light and all interactions that occur inside a scattering material are fully described by the following differential equation, known as the radiative transport equation (RTE):

$$(\vec{\omega} \cdot \vec{\nabla})L(x, \vec{\omega}) = -\sigma_t L(x, \vec{\omega}) + \sigma_s \int_{4\pi} p(\vec{\omega}, \vec{\omega}') L(x, \vec{\omega}') d\omega' + Q(x, \vec{\omega})$$

Here,  $Q(x, \vec{\omega}) [W m^{-3}]$  is the source term describing the amount of light emitted from the point  $x$ . This term is used with the phenomenon of fluorescence for instance. We will not use it in our following study.

**Phase function:** The phase function is a normalized distribution, i.e.  $\int_{4\pi} p(\vec{\omega}, \vec{\omega}') d\omega' = 1$ . A barely restrictive hypothesis, which is not true in the general case, is the symmetry of the phase function:  $p(\vec{\omega}, \vec{\omega}') = p(\vec{\omega}', \vec{\omega})$ . In this case, the phase function only depends on the angle between  $\vec{\omega}$  and  $\vec{\omega}'$ , thus  $p(\vec{\omega}, \vec{\omega}') = p(\vec{\omega} \cdot \vec{\omega}')$ .

There exists some approximations as the Henyey-Greenstein phase function (HG) or the Rayleigh phase function. The Henyey-Greenstein phase function is the following:

$$p(\vec{\omega} \cdot \vec{\omega}') = \frac{1}{2} \frac{1 - g^2}{(1 + g^2 - 2g\vec{\omega} \cdot \vec{\omega}')^{3/2}}$$

This model has a parameter  $g \in [-1, 1]$  that represents the anisotropy of the phase function. An isotropic phase function is when  $g = 0$ , which distributes light equally in all directions. An interesting property of Henyey-Greenstein phase function is that all phase functions  $\phi$  can be approximated by an HG phase function by calculating  $g = \int_{4\pi} (\vec{\omega} \cdot \vec{\omega}') \phi(\vec{\omega} \cdot \vec{\omega}') d\omega'$ .

## 3.2 Related Work

The field of subsurface scattering is studied by researcher for over 50 years, with first works on neutron transport in material that is a totally equivalent situation to those of light transport. Until now, only a few methods have been recognized by the community. The simulation of subsurface scattering is an intricate problem. Moreover, there has not been found any analytical solution to the radiative transport equation due to its complexity.

There are two widely used techniques concerning the subsurface scattering, Monte-Carlo path tracing and the diffusion approximation. These techniques are the most common. The former is considered as the ground truth concerning rendering of subsurface scattering, and the latter is really fast to compute but is a coarse approximation. Other methods have been developed to replace Monte-Carlo and the diffusion approximation. However, none of these methods achieved to have much success.

### 3.2.1 Monte-Carlo Path Tracing

The Monte-Carlo path tracing determines illumination of the scene stochastically, using probabilistic algorithms. The principle is to determine the rays going from the camera to the source of light, following any possible path. Due to the geometrical nature of optics, this is an equivalent problem to the situation where rays are going from the light sources to the camera lens. That is to say that the paths of light are independent of the ray directions.

The method consists in throwing rays at random from the camera, for each pixel of the image. These rays are reflected, refracted, scattered, absorbed and so on, performing the different physical interactions with the scene. At each of these interactions, the light bounces and takes a new direction driven by probability density distribution for that interaction. In the case of refraction as an example, physics tells us that the ray will split in a reflected ray with a proportion of light intensity  $F_r$  and in a refracted ray with a proportion of light intensity  $1 - F_r$ ,  $F_r$  being the Fresnel reflection coefficient. In path tracing, each ray will choose only one of these two paths with the probability  $F_r$  and  $1 - F_r$ , respectively.

At the end of their path, the rays can either finish in the void, or reach a source of light. In the latter case, they will contribute to the final color of the pixel. The color of the pixel being the average color of all rays thrown from this pixel and that hit a light source. Then all these rays are gathered to compose the final image.

---

**Monte-Carlo method basics:** Monte-Carlo method works on the fact that we can calculate the integral of any function  $g$  by using random samples [4]. This property uses the definition of the expectation:

$$E[g(X)] = \int g(x)f_X(x)dx$$

with  $f_X$  the probability density function of the random variable  $X$ .

In general we take an uniform distribution  $X \sim \mathcal{U}(a, b)$ , so  $f_X(x) = \frac{1}{b-a}$ .

Then, choosing a sample  $(x_1, x_2, \dots, x_N)$  of the distribution of  $X$ , we can compute the expectation by the empirical mean:

$$E[g(X)] \simeq \frac{1}{N} \sum_{i=1}^N g(x_i)$$

Finally we can compute the integral of  $g$ :

$$\int_a^b g(x)dx \simeq (b-a) \frac{1}{N} \sum_{i=1}^N g(x_i)$$

This method also works in the general case. We can choose other sampling distribution than the uniform sampling to compute the integral. Modifying the distribution of the random variable  $X$  may be interesting. With a good distribution of  $X$  we can make the convergence of the Monte-Carlo method faster and also simplify the expression of  $g$ . This is called importance sampling:

$$\int g(x)dx = E \left[ \left( \frac{g}{f_X} \right) (X) \right] \simeq \frac{1}{N} \sum_{i=1}^N \frac{g(x_i)}{f_X(x_i)}$$

The Monte-Carlo path tracing technique is used as the ground truth for validating other methods because it simulates the entire and exhaustive behavior of light in materials. It converges to a perfect image asymptotically. However this has a major drawback. This probabilistic method only converges slowly as it needs a huge number of samples to converge. This results in an enormous computational time to obtain good looking pictures.

### 3.2.2 Diffusion Approximation

Jensen [6] introduced a technique to compute the subsurface scattering that is now the most widespread due to its high speed. Under some simplifications they manage to find an analytical solution of the radiative transport equation. This solution has the form of a diffusion-like equation.

To make that possible, they make some assumptions. They assume that there is an infinite number of scattering event when light interacts within the material. Actually, after a number of scattering event the light loses its directionality because each scatter event can be viewed as a convolution with the phase function, and this result in an effect of blurring. This explains the form of the solution as a diffusion approximation, as diffusion is a form of blurring.

They approximate the radiance by the two first terms of spherical harmonics, which gives them a distribution of radiance of low frequency:

$$L(x, \vec{\omega}) \approx \frac{1}{4\pi} \phi(x) + \frac{3}{4\pi} \vec{\omega} \cdot \vec{E}(x)$$

Here,  $\phi(x) = \int_{4\pi} L(x, \vec{\omega}) d\omega$  is the scalar irradiance or fluence, and  $\vec{E}(x) = \int_{4\pi} L(x, \vec{\omega}) \vec{\omega} d\omega$  is the vector irradiance.

Under this approximation they find an analytic solution to the radiative transport equation under the form of the following diffusion-like equation:

$$D\nabla^2 \phi(x) = \sigma_a \phi(x) - Q_0(x) + 3D\vec{\nabla} \cdot \vec{Q}_1(x)$$

Here,  $Q_0(x) = \int_{4\pi} Q(x, \vec{\omega}) d\omega$  and  $\vec{Q}_1(x) = \int_{4\pi} Q(x, \vec{\omega}) \vec{\omega} d\omega$ .  $D = \frac{1}{3\sigma'_t}$  is the diffusion constant, where  $\sigma'_t = \sigma_a + \sigma'_s$  and  $\sigma'_s = \sigma_s(1-g)$ .

They resolve this diffusion-like equation by a dipole: they place two sources of light, one real and one virtual, at location  $z_r = 1/\sigma'_t$  and  $z_v = z_r + 4AD$  below and above the surface, with  $A$  another constant developed in the article. This gives them the diffuse reflectance

$$R_d(r) = \frac{\alpha'}{4\pi} \left[ \frac{z_r(\sigma_{tr}d_r + 1) e^{-\sigma_{tr}d_r}}{d_r^2} \frac{1}{d_r} - \frac{z_v(\sigma_{tr}d_v + 1) e^{-\sigma_{tr}d_v}}{d_v^2} \frac{1}{d_v} \right]$$

where  $d_r = \|x - x_r\|$  is the distance to the real source and  $d_v = \|x - x_v\|$  is the distance to the virtual source. Finally they obtain a formula for BSSRDF

$$S_d(x_i, \vec{\omega}_i, x_o, \vec{\omega}_o) = \frac{1}{\pi} F_t(\eta, \vec{\omega}_i) R_d(\|x_i - x_o\|) F_t(\eta, \vec{\omega}_o)$$

where  $F_t$  are the Fresnel transmission coefficients.

### 3.2.3 Overview of Other Methods

There exists other methods in this field but they meet little success compared to the two previous ones. They will be explained in this section.

**Analytic multiple scattering:** In the article of Narasimhan [7] they find an analytical solution to the transport equation in the form of a Legendre polynomial decomposition. They place themselves in the case of an isotropic source of light, i.e. the light is emitted equally in all directions. The source of light is at the center of a sphere filled with the studied material. Under these conditions there is a spherical symmetry.

Thus they can simplify the expression of radiance as being  $L(T, \mu)$  and only take two coordinates  $T$  as the radius position in the sphere and  $\mu$  as cosine of the outgoing light angle. They also make the assumption of separability:  $L(T, \mu) = g(T)f(\mu)$ . Finally, they obtain the simple solution

$$L(T, \mu) = \sum_{m=0}^{\infty} [g_m(T) + g_{m+1}(T)] L_m(\mu)$$

where  $L_m$  are Legendre polynomials and

$$g_m(T) = L_0 \exp \left[ -\frac{2m+1}{m} \left( 1 - \frac{(2m+1)g^m - 1}{2m-1} \right) T - (m+1) \log T \right]$$

**Empirical BSSRDF:** Donner [3] uses an empirical method to compute the scattering. In this article they place themselves in the case where the light beam hits a semi-infinite plane. Their method is intended to use a precomputation of the 12D BSSRDF function, i.e. 8D plus 4 parameters:  $S(x_i, \vec{\omega}_i, x_o, \vec{\omega}_o | \sigma_s, \sigma_a, g, \eta)$ .

They precompute this BSSRDF in a large table and intend to use this table to directly compute the scattering of the objects in the final scene. Because of the offline nature of this precomputing, they can obtain very precise values by using the Monte-Carlo technique during a long time (several month in their case).

In order to reduce the size of the table, they first reduce the number of parameters by exploiting some correlations. They replace  $(x_i, \vec{\omega}_i = (\theta_i, \phi_i), x_o, \vec{\omega}_o = (\theta_o, \phi_o), \sigma_s, \sigma_a, g, \eta)$  by  $(\theta_i, r =$

$\|x_o - x_i\|, \theta_s, \theta_o, \phi_o, \alpha, g, \eta$ ). Secondly they approximate the exiting lobes, i.e. the two dimensions ( $\theta_o, \phi_o$ ), by fitting custom-made ellipses. Finally, the remaining dimensions ( $\theta_i, r, \theta_s, \alpha, g, \eta$ ) are sampled over 10 samples per parameter around.

At the end, and with all these optimizations, they obtain a huge 250MB dataset to represent every BSSRDF for parameters varying in their range.

**Dirac phase function:** Vitkin [10] explores the idea of decomposing the phase function in two parts, one directional and the other non-directional:

$$p(\vec{\omega} \cdot \vec{\omega}') = p_{DI}(\vec{\omega} \cdot \vec{\omega}') + [p(\vec{\omega} \cdot \vec{\omega}') - p_{DI}(\vec{\omega} \cdot \vec{\omega}')] ]$$

where  $p_{DI}$ , composed of a Dirac function, is the directional part:

$$p_{DI}(\vec{\omega} \cdot \vec{\omega}') = \frac{1}{4\pi} [1 - g + 2g\delta(1 - \vec{\omega} \cdot \vec{\omega}')] ]$$

This decomposition brings the radiative transport equation to be separable:

$$\begin{aligned} (\vec{\omega} \cdot \vec{\nabla})L(x, \vec{\omega}) = & -\sigma'_t L(x, \vec{\omega}) \\ & + \frac{\sigma'_s}{4\pi} \int_{4\pi} L(x, \vec{\omega}') d\omega' \\ & + \sigma_s \int_{4\pi} [p(\vec{\omega}, \vec{\omega}') - p_{DI}(\vec{\omega}, \vec{\omega}')] L(x, \vec{\omega}') d\omega' \end{aligned}$$

From this equation they find logical to decompose the radiance into three different parts:

$$L(x, \vec{\omega}) = \underbrace{L_d(x, \vec{\omega})}_{\text{diffuse part}} + \underbrace{L_p(x, \vec{\omega})}_{\text{phase dependant part}} + \underbrace{L_c(x, \vec{\omega})}_{\text{collimated part}}$$

Under the hypothesis of a semi-infinite plane that is striked by a narrow collimated vertical beam of light, solving the RTE with these three parts run into an analytical solution for  $L(x, \vec{\omega})$  as the sum of the two following equations. The first equation represents the diffuse light and is analogous to the diffusion approximation:

$$R_d(\rho) = \frac{\sigma'_s}{4\pi} \int_0^\infty \left[ z \frac{1 + \sigma_{tr} r_1}{r_1^3} e^{-\sigma_{tr} r_1} + \left( z + \frac{4}{3\sigma'_t} \right) \frac{1 + \sigma_{tr} r_2}{r_2^3} e^{-\sigma_{tr} r_2} \right] e^{-\sigma'_t z} dz$$

The second equation is the phase function correction term that describes the behavior of light near the source:

$$R_p(\rho) = \sigma_s \int_0^\infty \left[ p\left(\frac{-z}{r}\right) - \frac{1-g}{4\pi} \right] \frac{z}{r_1^3} e^{-\sigma'_t(z+r_1)} dz$$

Here,  $r_1 = \sqrt{\rho^2 + z^2}$  and  $r_2 = \sqrt{\rho^2 + (z + 4/3\sigma'_t)^2}$ .

This method results in a better accuracy near the source of light than the diffusion approximation.

**Quantized-diffusion:** In the article of d'Eon [2], they place themselves in the case of the layered searchlight problem: This problem is modeled by a layered scattering material illuminated by a vertical beam of light, and is to find the radiance reflected and transmitted at each location and for each direction on the surface.

They propose a modified version of the theory behind the diffusion approximation and they use improved boundary conditions to solve the diffusion equation. Then, to compute the

diffusion reflectance, they use what they call quantized diffusion, which is a sum of Gaussians. This sum of Gaussians is applied under the form of a multipole, which extends the dipole of the classical diffusion approximation. With the multipole, series of positive and negative light source are placed above and below the surface of the material.

The advantage of their method is that they can use thinner layers of material than other methods and remain accurate.

**Better dipole:** D'Eon [1] shows an improvement of the diffusion approximation by only modifying the parameters of the final solution. This modification is based on different boundary conditions from the initial diffusion approximation ones. The new resulting formula for the diffusion reflectance become:

$$R_d(r) = \frac{\alpha'^2}{4\pi} \left[ \left( C_{\bar{E}} \frac{z_r(\sigma_{tr}d_r + 1)}{d_r^2} + \frac{C_\phi}{D} \right) \frac{e^{-\sigma_{tr}d_r}}{d_r} - \left( C_{\bar{E}} \frac{z_v(\sigma_{tr}d_v + 1)}{d_v^2} + \frac{C_\phi}{D} \right) \frac{e^{-\sigma_{tr}d_v}}{d_v} \right]$$

where  $C_\phi = \frac{1}{4}(1 - 2C_1)$  and  $C_{\bar{E}} = \frac{1}{2}(1 - 3C_2)$ . The other changes occur in the definition of the two constants  $A$  and  $D$ :

$$A = \frac{1 + 3C_2}{1 - 2C_1} \quad D = \frac{2\sigma_a + \sigma'_s}{3(\sigma_a + \sigma'_s)^2}$$

Here, the constants  $C_1$  and  $C_2$  come directly from Quantized-diffusion [2].

# Simulation and Analysis of Scattering Materials

In the previous work there is no simple method that has only advantages. On one hand Monte-Carlo is too expensive in computing time. On the other hand, the diffusion approximation fails to characterize highly anisotropic materials, and even for isotropic materials this cannot describes the behavior of light near the source. Finally, the other methods are either too complex or too expensive in term of memory.

We are looking for a technique having the simplicity of the diffusion approximation and the accuracy of the Monte-Carlo path tracing for anisotropic materials. We plan to limit ourselves to the configurations where the diffusion approximation fails. Our objective is to create an hybrid method composed of the diffusion approximation where diffusion works and our own method where diffusion fails.

## 4.1 Study of the Behavior of Diffusion Approximation

Our first objective is to understand how behaves the diffusion approximation compared to Monte-Carlo, where the approximations made for the diffusion are good enough and in what conditions. With this understanding we thus can limit ourselves to the parts where diffusion fails.

We have developed a program that simulate light scattering in a volume of material. The resulting data will be the center of our following work.

**Description of our simulation:** This program simulates a beam of light entering the scattering material at the origin of the world. All the space is filled with material and the incoming light will be subject to several scattering events before being absorbed. The simulation uses the Monte-Carlo method to compute the scattering. We use the Henyey-Greenstein formula as the phase function.

We sample the space of  $L(x, \vec{\omega})$  by four parameters (see Figure 4.1) into bins. Two parameters are the cylindrical coordinates  $r \in [0, 1.5]$  and  $z \in [-1, 3]$ , normalized so that their unit is the mean free path. We get rid of the third angular coordinate of the cylindrical coordinates because the symmetry existing around the entering beam of light makes this parameter superfluous. The two other parameters are  $\theta \in [0, \pi]$  and  $\phi \in [0, 2\pi]$ , the direction of light.

At each scattering event, the contribution of light is computed and added to the corresponding bin. We can change quantities as  $g$  and  $\alpha$  to account for a different scenario. Finally, the

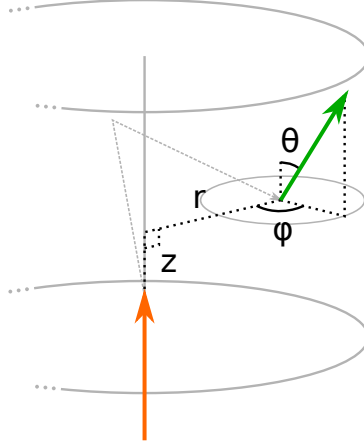


Figure 4.1: *Setup of our simulation. The orange arrow represents the beam of light. The green arrow represents the sampled light. The beam of light is entirely immersed inside the material. Its source is at coordinates  $(r,z) = (0,0)$ .*

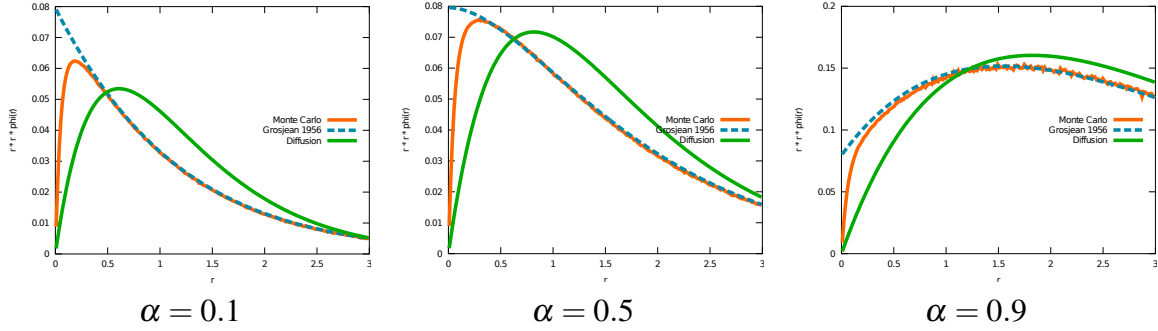


Figure 4.2: *Fluence  $\phi$  for an isotropic phase function ( $g = 0$ ). The graphs show  $r^2\phi(r)$  with respect to  $r$ . Compared to our simulation that is the ground truth (orange), the diffusion approximation (green) tends to underestimate the amount of light near the source (at less than  $1mfp$ ), but it overestimates the amount of light further away. Grosjean approximation (blue) is closer to our simulation than the diffusion, but also fails very near the source.*

resulting dataset is stored in a file to be later analysed.

**Discussion around the diffusion approximation:** First, as an indication of the correctness of our simulation, we have retrieved the same results as those of d’Eon [2]. When computing the fluence  $\phi(x)$  in isotropic material, we obtain the results shown on Figure 4.2 for different albedos. Our simulation is in orange, the fluence from diffusion approximation is in green and Grosjean approximation is in blue [5].

We can see on Figure 4.2 that the diffusion approximation tends to underestimate the amount of light near the source (when  $r < 1mfp$ ) and overestimates the amount of light further away. Grosjean approximation is better than the diffusion approximation but also fails at short distance from the source.

Next, we compare the real vector irradiance  $\vec{E}(x) = \int_{4\pi} L(x, \vec{\omega}) \vec{\omega} d\omega$  and the vector irradiance  $\vec{E}(x) = -D\vec{\nabla}\phi(x)$  computed with the equation from the diffusion approximation. We can see that in the case of anisotropic materials, these two quantities are varying widely. In Figure

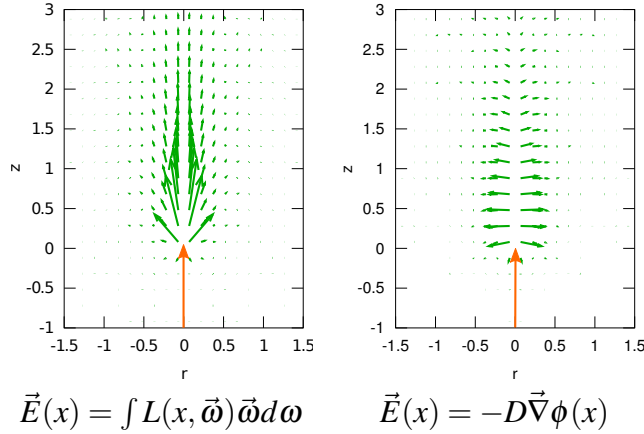


Figure 4.3: Comparison between vector irradiance (green arrows) in the case of anisotropy, where  $g = 0.9$ . Real  $\vec{E}$  is shown on the left and  $\vec{E}$  from diffusion approximation on the right. The orange arrow represents the source of light. Real  $\vec{E}$  tends to follow the direction of the light beam unlike  $\vec{E}$  from diffusion approximation which is perpendicular to the beam of light, even near the source.

4.3 the material is highly anisotropic, as  $g = 0.9$ . On one side the real  $\vec{E}$  tends to follow the beam of light, so it is relatively in the same direction as of incident light. On the other side the diffusion approximation  $\vec{E}$  seems perpendicular to the incident light, due to being originating from a gradient, which tends to blur some parts of the vector field (as rotational part for instance). This shows that the diffusion approximation is in this case far from reality. As previously mentioned, the error is more important near the source of light with the fluence and also with the vector irradiance.

A remark concerning the albedo  $\alpha$  is that the number of scattering events follows a geometric distribution  $\mathcal{G}(\alpha)$ , as at each scattering event, a ray has a probability of  $\alpha$  to be scattered and  $1 - \alpha$  to be absorbed. This means that the average number of scattering events for a particular material will be  $1/\alpha$ . Then, the configurations where  $\alpha \ll 1$  involve a lot of scattering events on average, because  $1/\alpha$  will tend to infinity. When there are a lot of scattering events, we get closer to the hypothesis of infinite number of scattering event. Thus, this is the case where diffusion approximation becomes good, so we will exclude this situation in our model.

## 4.2 Finding a Better Description

From this analysis, we want to find a model that will describe  $L(x, \vec{\omega})$  better, near the source of light in particular (i.e. of the order of the mean free path). We do not restrict ourselves to a model based on a theoretical study and reserves the right to create an empirical model. In this context we have tried several different models with more or less results.

To find our model as described in the previous simulation, we choose to place ourselves in a different situation than previous work. In general, other methods place themselves at the interface of the material by modelling a semi-infinite plane. The light hits this interface within a certain configuration. Unlike these methods, we place ourselves inside the medium, as all the space is filled with material. The light is already immersed in the material, even its source. This allows us to discard the effect of refraction at the interface. Furthermore, as other methods

use planar surface for refraction, they can't have non-planar surfaces without adding errors. We can take this advantage to use every kind of surface we want, which is important because the surfaces are very rarely planar in practice. Thus we are treating a more general case.

## 4.2.1 Spherical Gaussian Approximation

The first model studied is based on spherical Gaussians. With this model we want to approximate the directional part of  $L(x, \vec{\omega})$ , that is to say we want to approximate the lobes at each position  $x$ . The lobes represent  $L$  for all directions  $\vec{\omega}$ .

Our first attempt is to approximate each lobe by a spherical Gaussian because this is a function which looks like a lobe. This function is leaving us with three parameters that will only depend on the location in space.

---

**Spherical Gaussians:** A spherical Gaussian (SG) is a function of the form:

$$G(\vec{v} \mid \vec{p}, \lambda, \mu) = \mu e^{\lambda(\vec{v} \cdot \vec{p} - 1)}$$

where:

$$\begin{aligned} \vec{v} &\in \mathbb{S}^2 \\ \vec{p} &\in \mathbb{S}^2 & \vec{p} \text{ is the direction of the SG} \\ \lambda &\in \mathbb{R}^+ & \lambda \text{ is the sharpness of the SG} \\ \mu &\in \mathbb{R} & \mu \text{ is the amplitude of the SG} \end{aligned}$$

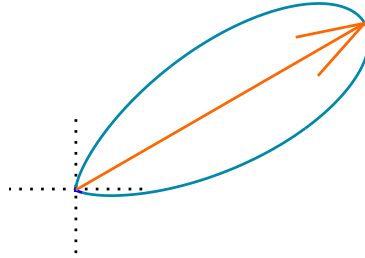


Figure 4.4: Example of a spherical Gaussian shape with the following parameters:  $\vec{p} = (\cos \frac{\pi}{3}, \sin \frac{\pi}{3})^T$  as the orange arrow,  $\lambda = 10$ ,  $\mu = 1$ .

Spherical Gaussians have good properties [11]. The product of two SGs is another SG:

$$G(\vec{v} \mid \vec{p}_1, \lambda_1, \mu_1) G(\vec{v} \mid \vec{p}_2, \lambda_2, \mu_2) = G(\vec{v} \mid \frac{\vec{p}_m}{\|\vec{p}_m\|}, \lambda_m \|\vec{p}_m\|, \mu_1 \mu_2 e^{\lambda_m (\|\vec{p}_m\| - 1)})$$

The inner product has also an analytical solution:

$$G_1 \cdot G_2 = \int_{\mathbb{S}^2} G(\vec{v} \mid \vec{p}_1, \lambda_1, \mu_1) G(\vec{v} \mid \vec{p}_2, \lambda_2, \mu_2) dv = \frac{4\pi \mu_1 \mu_2}{e^{\lambda_m}} \frac{\sinh(\lambda_m \|\vec{p}_m\|)}{\lambda_m \|\vec{p}_m\|}$$

Here,  $\lambda_m = \lambda_1 + \lambda_2$  and  $\vec{p}_m = \frac{1}{\lambda_m} (\lambda_1 \vec{p}_1 + \lambda_2 \vec{p}_2)$ .

In our case we want to find an approximation by  $L(x, \vec{\omega}) = G(\vec{\omega} | \vec{p}(x), \lambda(x), \mu(x))$ . This model does not permit us to find an analytical solution to the radiative transport equation. Thus we finally opt for an empirical solution.

To view what happens in practice, we take the data of our simulation with the values  $g = 0.9$  and  $\alpha = 0.5$ , and we compute a fitting of spherical Gaussian for each sample position in the volume. This fitting is done with the method of Gauss-Newton. We estimate only the two parameters  $\lambda$  and  $\mu$ . The estimation of  $\vec{p}$  is not computed with the Gauss-Newton method because this method is unstable in that case. However we choose the vector irradiance  $\vec{E}$  as an estimation of  $\vec{p}$ , which reveals to be a good estimation.

We obtain the results shown on Figure 4.5. To show the lobes, we place ourselves in the plane corresponding to all the directions where  $\phi = 0$ . This cutting plane is the symmetrical plane of the lobes by construction. Moreover, hatchings are drawn on the displayed lobes to indicate the interior of these lobes. This is done in order to account for negative values of radiance. Indeed, if  $L(x, \vec{\omega}) = -L(x, -\vec{\omega})$  then these two amplitudes will be displayed at the same point, so hatchings are there to distinguish them. Hatchings towards the center of the lobe indicate positive values as hatchings in the inverse direction indicate negative values.

We can see that the lobes are highly directional. The spherical Gaussians appear to approximate well the lobes in this direction, which is the “specular” part of the lobes. However, in the other directions, spherical Gaussian does not fit well to the lobe, as shown in Figure 4.5 (b). In general, spherical Gaussians tend to underestimate the lobes.

Another problem is that lobes are often flattened in the  $\phi = 0$  plane (see Figure 4.6). As we go away from the source, this flattening is less and less perceptible.

This model comes with some limitations. The spherical Gaussians cannot handle the flattening of the lobes because they have a circular symmetry around their axis by definition. This results in spherical Gaussians that are underestimating the lobe in the plane  $\phi = 0$ , as we can see for several lobes in Figure 4.5. In the other directions, the SGs are overestimating the lobes. This behavior is shown in Figure 4.6.

Another limitation is that spherical Gaussians do not approximate well the “diffuse” part of each lobe. The “diffuse” part meant to be the part of radiance in all other directions than the “specular” part. As we can see in Figure 4.7, this “diffuse” part is not approximated by the spherical Gaussian.

As shown in Figure 4.7, the “diffuse” part is clearly not constant, so we can’t approximate it by a constant, as in the Lambert model for instance, to account for the “diffuse” contribution.

## 4.2.2 Double Exponential Approximation

The limitation of the spherical Gaussian model concerning the “diffuse” part has conducted us to find a second model. As spherical Gaussians poorly approximate the lobes, we want to know if there emerges another model from the view of the lobe curves in the  $\phi = 0$  plane:  $L(\vec{\omega} = (\theta, 0))$  with respect to  $\theta$ .

As with spherical Gaussians, we use the dataset created from our simulation with  $g = 0.9$  and  $\alpha = 0.5$ . We notice that these curves have values varying widely, which makes them difficult to clearly understand their shape. Thus we pass in the log space. In this space, the curve seems to have an exponential shape. After doing some trial, we have finally found an empirical expression for  $L$  with a double exponential that approximate well the true radiance (see Figure 4.8). We can see that the model succeeded to approximate as much the peak of radiance, the “specular” part, as the bottom of the curve, the “diffuse” part.

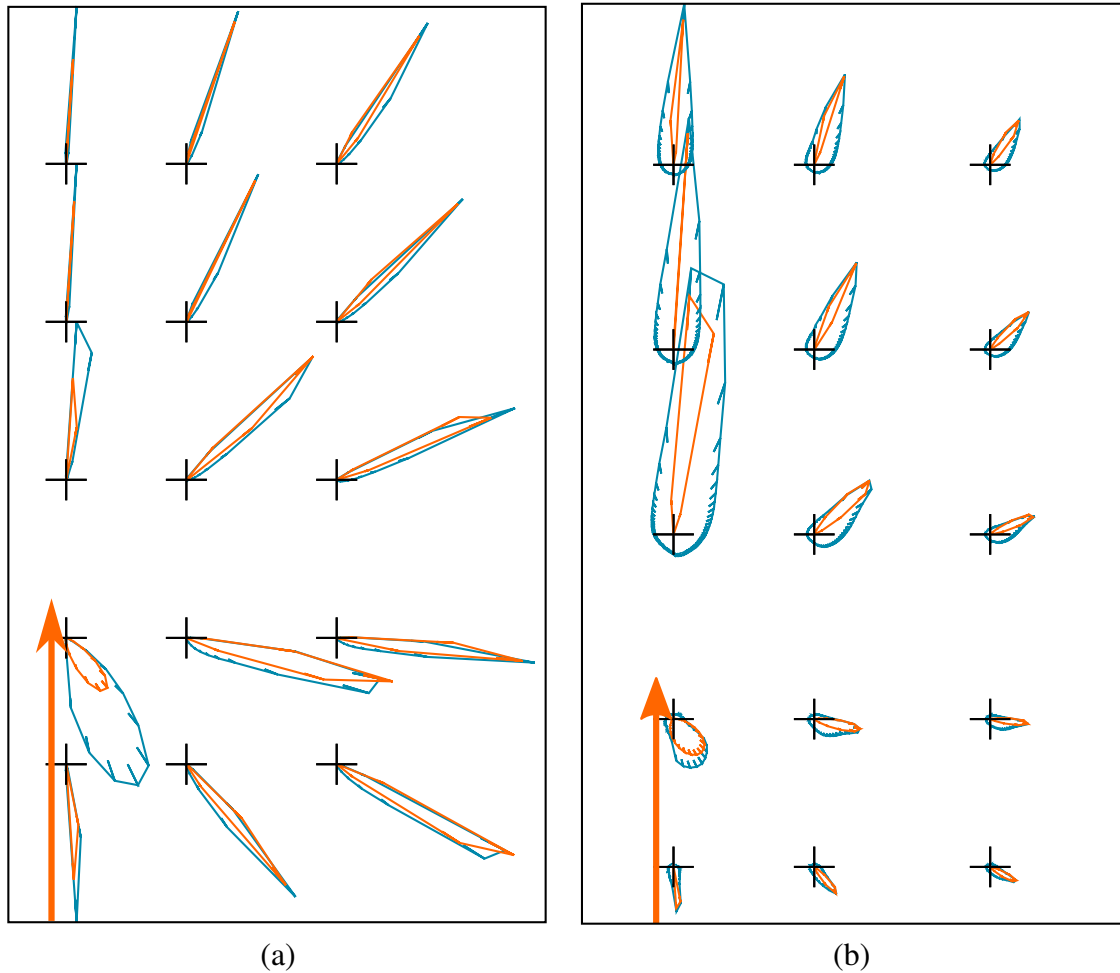


Figure 4.5: Several lobes of radiance at different locations. The locations are separated by around  $0.75\text{mfp}$ . The 2D lobes are a cut in the plane  $\phi = 0$  of the initial 3D lobes. The true radiance is shown in blue and the spherical Gaussian fit in orange. The arrow represents the entering beam of light. (a) True shape of the lobes. However, because of the great difference of amplitude between the lobes, each one is scaled by a constant to be displayable. (b) Deformed shape of the lobes: the lobes are displayed with an amplitude of  $\sqrt[4]{L}$  instead of just  $L$ , for a better view. We can see that the spherical Gaussians approximate poorly the “diffuse” part of each lobe.

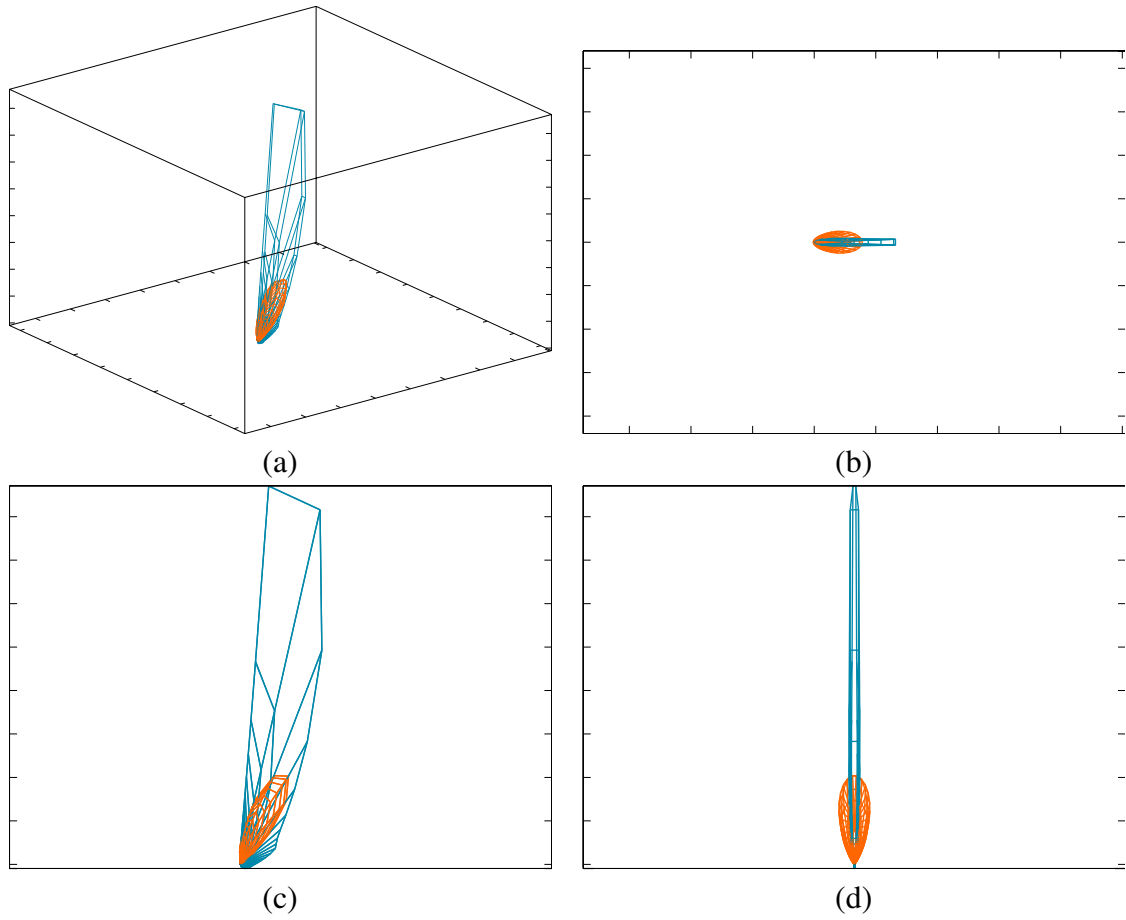


Figure 4.6: *The 3D lobe at location  $(r,z) = (0.075,0)$  shown from different points of view. The true radiance is in blue and the spherical Gaussian in orange. The spherical Gaussian does not handle the flattening of the lobe. (a) Perspective. (b) XY plane. (c) XZ plane, i.e. the  $\phi = 0$  plane. (d) YZ plane.*

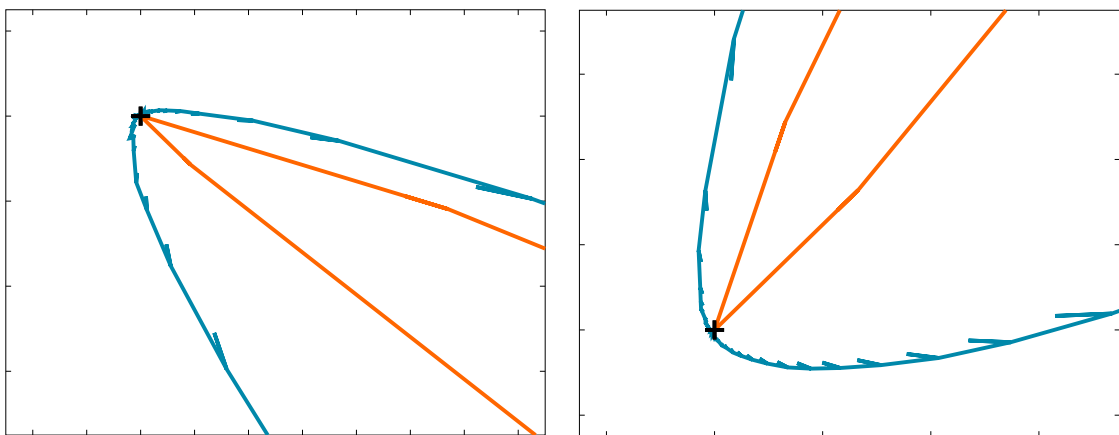


Figure 4.7: *Closeup of the “diffuse” part of some lobes in the  $\phi = 0$  plane. The true radiance is in blue and the spherical Gaussian in orange. Spherical Gaussians are poorly approximating the “diffuse” part of the lobes, as they largely underestimate it.*

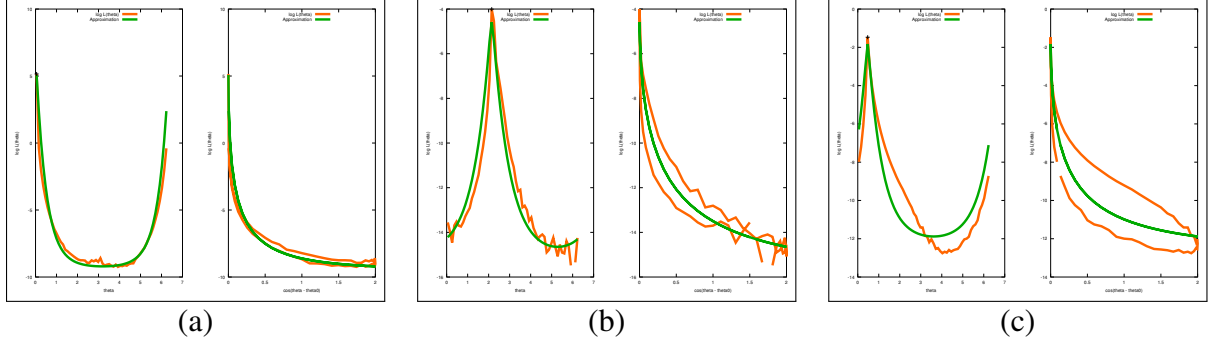


Figure 4.8: *Source of the intuition for our second model: graphs of  $L(\vec{\omega} = (\theta, 0))$  for three different lobes. For each lobe, there is represented a couple of graphs: there is displayed a plot of  $\log L(\theta)$  with respect to  $\theta$  on the first graph and a plot of  $\log L(\theta)$  with respect to  $1 - \cos(\theta - \theta_0)$  on second graph.  $\theta_0$  is defined by  $L(\theta_0)$  being the peak of each lobe. The orange curves are the real values of  $L$  and the green curves are our double exponential model. Our model fits well the real curves. (a) Lobe at coordinates  $(r, z) = (0, 2.9)$ . (b) Lobe at coordinates  $(r, z) = (1.5, -1.1)$ . (c) Lobe at coordinates  $(r, z) = (1.5, 2.9)$ .*

Our double exponential model is the following:

$$L(x, \vec{\omega}) = \alpha(x) \exp \left[ \beta(x) e^{\gamma(x) \sqrt{1 - \vec{p}(x) \cdot \vec{\omega}}} \right]$$

Here,  $\vec{p} = (\theta_0, 0)$  represents the direction of the peak of  $L$ .

Because of the complexity of this expression, we were not able to derive the radiative transport equation using this equation. Thus we turn once again to an empirical estimation of each parameters  $\alpha$ ,  $\beta$ ,  $\gamma$  and  $\vec{p}$ .

The estimation is done in several steps:

1. We begin with  $\vec{p}$ . It is estimated by taking the direction of the peak of each lobe, that is to say to maximum value of  $L$ , which also gives us the value  $M = L(\vec{p}) = \max_{\vec{\omega} \in \mathbb{S}^2} L(\vec{\omega})$ . The equation of our model also results in the following identities:

$$\log L = \log \alpha + \beta e^{\gamma \sqrt{1 - \vec{p} \cdot \vec{\omega}}} \quad \text{and} \quad \log M = \log \alpha + \beta$$

2. Then,  $\gamma$  is estimated using

$$\gamma = 2 \log \left[ \frac{\log L(\vec{\omega}_2) - \log L(\vec{\omega}_1)}{\log L(\vec{\omega}_1) - \log M} \right] \quad \text{with} \quad \vec{p} \cdot \vec{\omega}_1 = \frac{3}{4} \quad \text{and} \quad \vec{p} \cdot \vec{\omega}_2 = 0$$

3. We estimate  $\log \alpha$  by a linear regression based on the following linear equation:

$$\left[ \log L - \log(M) e^{\gamma \sqrt{1 - \vec{p} \cdot \vec{\omega}}} \right] = \log \alpha \left[ 1 - e^{\gamma \sqrt{1 - \vec{p} \cdot \vec{\omega}}} \right]$$

4. Finally  $\beta = \log M - \log \alpha$ .

The results of this estimation are shown in Figure 4.9. We can see that  $\alpha$ , which represents the amplitude of the lobe, as high value in the ballistic direction of the entering light beam and

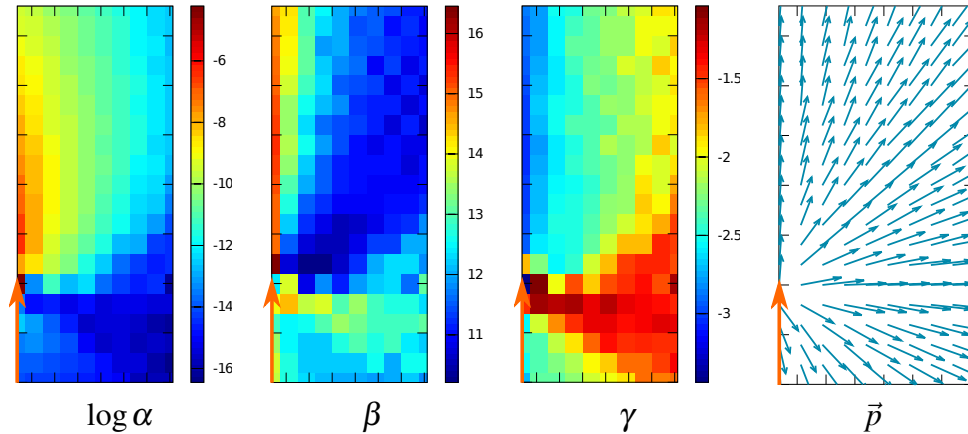


Figure 4.9: *Results of the estimation of the parameters. These images cover the spatial dimensions  $(r, z)$  of the dataset. The orange arrow identifies the entering beam of light.*

tends to fade with the distance to the source. The vector field of  $\vec{p}$  is close to the real vector irradiance  $\vec{E}$  previously shown in Figure 4.3. However the parameters  $\beta$  and  $\gamma$  have no intuitive explanation.

With the double exponential model, the resulting lobes are shown on Figure 4.10. This approximation has the same limitation than the spherical Gaussians concerning the flattening of the lobes. Because this model was created by only taking into account a 2D representation of each lobe, the approximation is not good anymore outside of the  $\phi = 0$  plane. This is because this model is circular around its axis, just as spherical Gaussians. However, the “diffuse” part is this time well approximated as we can see on Figure 4.10 (b). This model achieves being highly directional in the “specular” direction as well as being exact in the “diffuse” part.

### 4.3 Ray Tracer

We have also implemented a ray tracer, which represents about a thousand of lines of code. The objective is to visualize the behavior of the different methods in a practical situation, as well as to understand the concept underneath the complete pipeline of rendering of pictures. In this ray tracer, we have implemented the Monte-Carlo path tracing as reference.

Our ray tracer takes as input a scene composed of objects filled with different types of material. Then using a rendering method, the program outputs concrete images of the scene. The ray tracer accept two types of lighting: beams of light that are represented by a single ray of light, and area lights that are solid object emitting light. As material we can use the ones among materials described in the articles of Jensen [6] and Narasimhan [8].

The resulting pictures of our ray tracer can be seen in Figures 4.11, 4.12 and 4.13. On Figure 4.11 is shown scenes illuminated with a light beam. On Figure 4.12 and 4.13, the scenes are illuminated by a sphere. We can see the effects of scattering on the borders of the cubes which are brighter than the rest of the surface, as there is some light that passes through the object. For the sphere of milk, the scattering tends to illuminate the floor under the sphere, compared to the sphere of diluted orange powder.

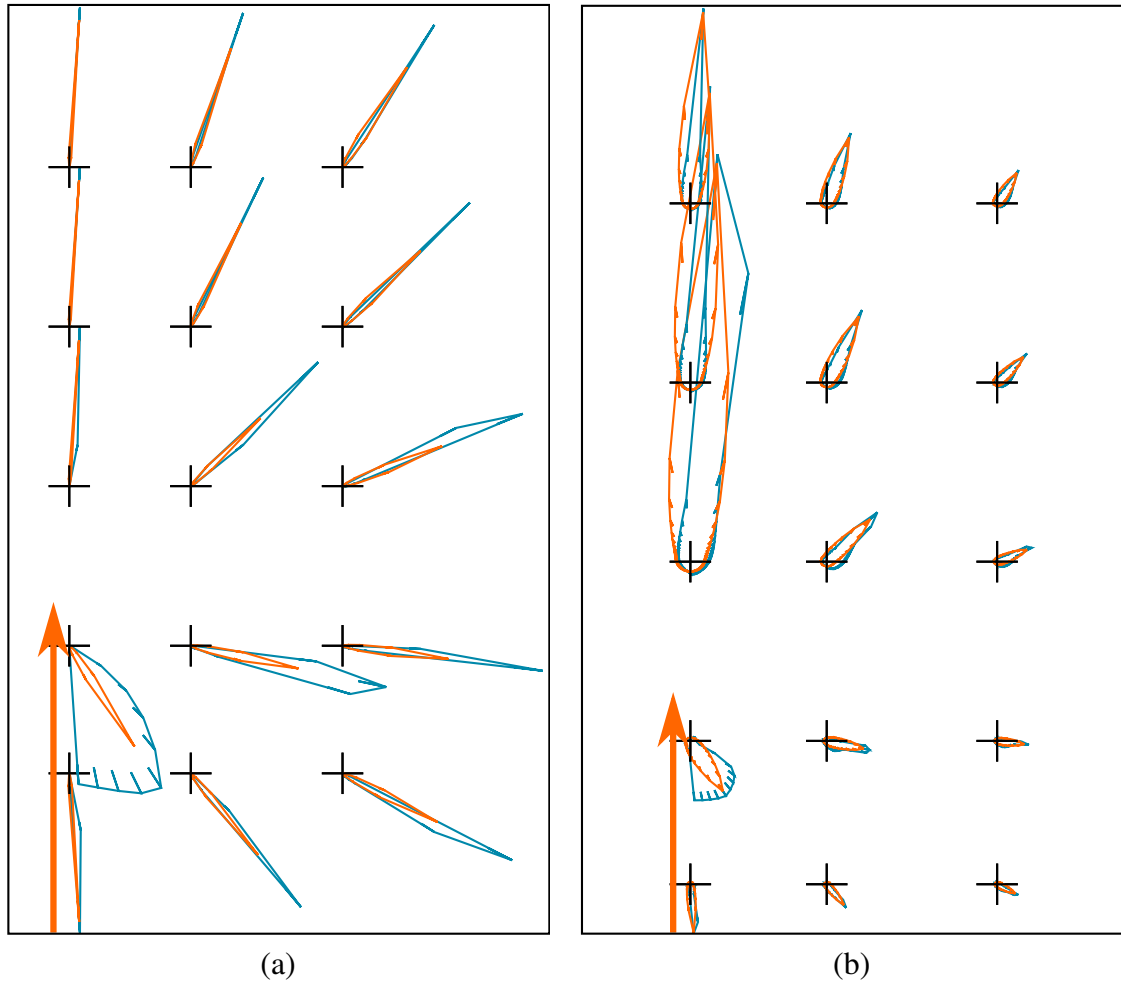


Figure 4.10: Several lobes of radiance at different locations, in the same configuration as in Figure 4.5. The true radiance is shown in blue and the double exponential approximation in orange. The double exponential model approximates well the “specular” and the “diffuse” parts. (a) True shape of the lobes, scaled by a constant. (b) Deformed shape of the lobes, displayed with an amplitude of  $\sqrt[4]{L}$ .

## 4.4 Validation

First, concerning our simulation that creates the datasets used as reference during the development of our two models, we compare against the results of d’Eon [2]. To do this, we take an isotropic medium configuration ( $g = 0$ ) to be in the same configuration as them. We then compute the radial fluence  $\phi(r)$  and when comparing against d’Eon, our data agrees with their results as we retrieve the same graphs.

Next, we suggest guides for validation of our models. Implementing our models in our ray tracer will permit us to compare them against the ground truth, which is the Monte-Carlo method. Then we can also implement our models in a well known existing software, like Mitsuba renderer for instance. This permit us to compare our technique against other techniques as the diffusion approximation for instance, as being already implemented by their respective authors, which testify for their correctness.

There are two measuring criteria that can be used for the comparison: a quantitative and a

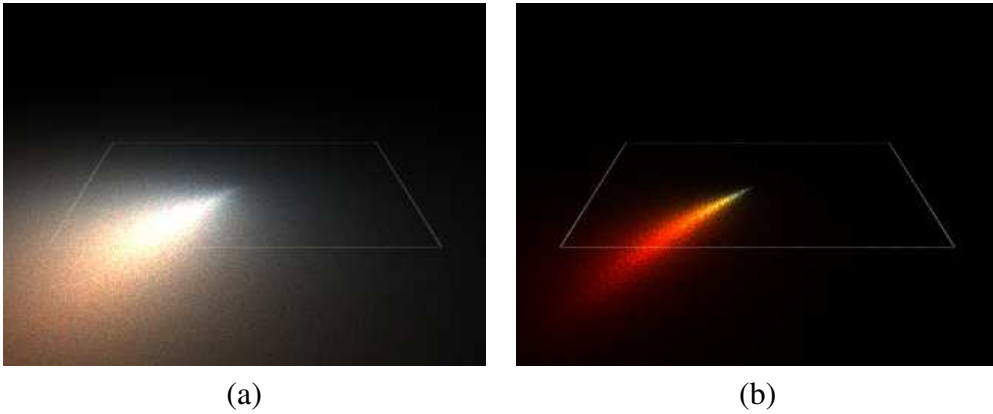


Figure 4.11: *Pictures showing the effect of scattering. These pictures are two semi-infinite planes illuminated by a beam of light hitting the surface with an oblique angle. The rectangles are 8 mean free path long. The scattering effect produces a halo around the incident beam of light. (a) The semi-infinite plane is filled with the material “milk (regular)” from Narasimhan [8]. (b) Here, the material used is “orange powder” also from Narasimhan [8].*

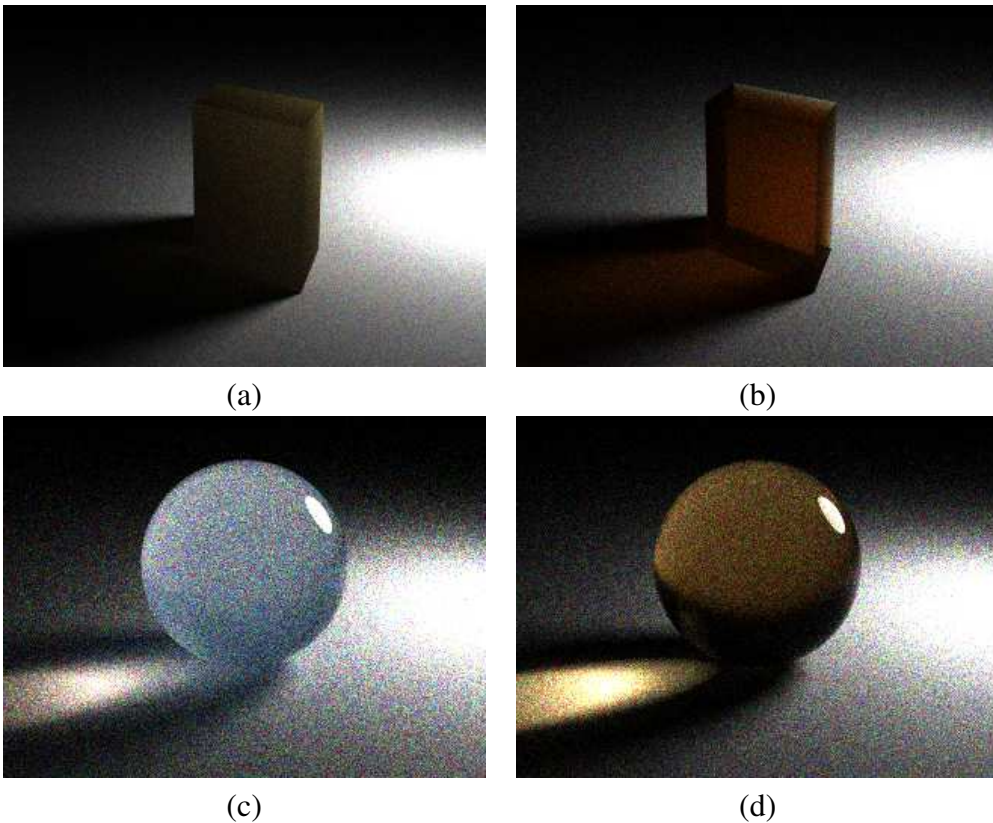


Figure 4.12: *Images of different objects illuminated by a sphere of light. All the filling materials come from Narasimhan [8]. The images are often noisy because the Monte-Carlo method takes too long time to converge. (a) A deformed cube of apple. (b) A deformed cube of diluted orange powder. (c) A sphere of milk. (d) A sphere of diluted orange powder. We can see the effect of scattering on the borders of the cubes, as light passes through them. On image (c) the floor is brighter under the sphere because of scattering.*

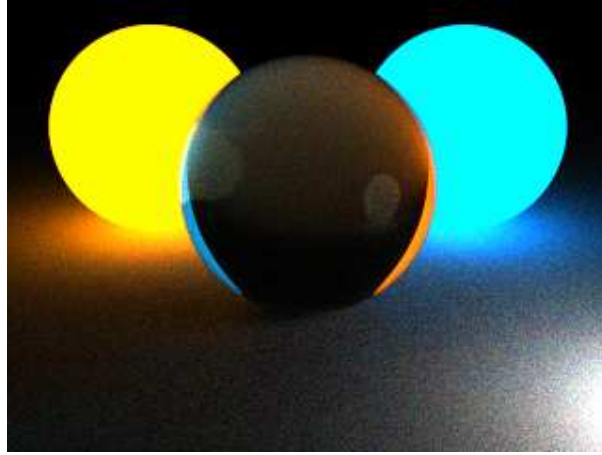


Figure 4.13: *Example of a more complex scene.*

qualitative measurement. The quantitative measurement will be to measure the differences in radiance between rendered pictures with our technique and rendered picture with other techniques, and Monte-Carlo in particular, to precisely know the committed error. Moreover we can make real measurements to complete this validation: a protocol could be to illuminate with a laser a sample of chosen scattering material that has not necessarily a planar surface. We take photographs of this sample with a camera at a certain angle. Then we compare these photographs to rendered pictures of a virtual scene. The scene will be created with a beam of light representing the laser, an object having the same shape, and the exact camera configuration.

The qualitative measurement, for its part, will be to ask people what they think about the rendered images: do they see any difference between images rendered with our model and images rendered with the others techniques? Do they think that there is any improvement? This measurement is important in the sense that humans are the final link in the chain of pictures rendering, as they will view these pictures. This is what rendering is intended for: be viewed by humans. Thus their perception is actually the most adapted criteria for evaluating of our work, as we try to make pictures looking more realistic or plausible for them.

Finally, our ray tracer can be validated against other well known ray tracers, as Mitsuba for instance. A method could be to create the same scene in our ray tracer and in the Mitsuba software, with the same objects, lights and the same configuration of the camera. Then the rendered pictures from these two sources can be compared to see if there are any differences.

Another method of validation for the ray tracer would be using experimental data, as photograph of a real scene. We recreate the same scene in our ray tracer and compare if there is any difference between the photo and the rendered image. Also, this method allows us to compare the accuracy of the different rendering techniques against reality.

## 4.5 Future Work

The first direction we will follow is to extend the analysis of our data to the remaining dimensions. We will search for the spatial behavior of the parameters of our models. For the spherical Gaussians model, we will look for understanding how  $\vec{p}$ ,  $\lambda$  and  $\mu$  act spatially, and also for the parameters  $\alpha$ ,  $\beta$ ,  $\gamma$  and  $\vec{p}$  of the double exponential model. We will furthermore

comprehend the interaction of these parameters with the anisotropy factor  $g$  and albedo  $\alpha$ . This work will allow us to complete our models in order to make them integrable in rendering softwares.

Then the next directions will be to analyse the effects and the problems that lobe flattening can pose, if there are any. We will also search for an optimized way to compute the complex expression of the double exponential model. We may also go towards making algorithm for scattering being real-time, taking advantage of the highly parallel nature of these types of method, and processing the algorithm on the GPU.

Finally we will study the importance of single scattering effect, where the light is only subjected to one scattering event before outgoing the material. This effect is in general treated separately because of its highly directional nature which is considered as a problem.



## Personal Experience

During this master project, I have acquired some knowledge around the way research works. I have understood that research is based on exploration of unknown domains. This leads to the advantage of being free to choose in which direction to further study, but can also bring frustration when the study comes to nothing interesting and as substantial discoveries are hard to make. The work is mainly aimed to transmit knowledge by writing papers and giving talks at various meetings. Research is however not centered around the practical application part, of making ready to use products for instance.

Life within the team was great, because there were a good ambience. Time when we discuss together has an interesting value, as that often feeds our reflexion with good elements. The reading groups, during which we exposed interesting papers, were a good way to enlarge our comprehension concerning our domain. I was able to attend talks that expanded the reflexion to broader domains. I could also see the process of creating a project-team, also with its struggles.

This project allowed me to extend greatly my understanding of how light works and the underlying theory, as well as other concepts in the field of Computer Graphics more generally. I wish I had more time in order to further develop the models of our work. In particular, the perspective of parallelization of the algorithms would be attractive to experiment, to better understand this kind of methods.



## Conclusion

In this project we have addressed the problem of light interacting with scattering materials. This problem is to compute efficiently the amount of light outgoing from the surface of an illuminated object that have scattering properties. There exists two common techniques, the Monte-Carlo path tracing considered as the ground truth, and the diffusion approximation.

From this background, we place ourselves in the context of creating a improved model for the computing of scattering effect. We have created a complete simulation of scattering inside materials, in a more general case than previous methods. From the resulting data of this simulation, we have analysed the case of lobes, i.e. the directional part of light. This analysis can serve as a base for future works. Moreover, we have developed the beginning of a model for scattering from this analysis, in two different versions with spherical Gaussians approximation and double exponential approximation. We have also coded a ray tracer to have a complete pipeline for pictures rendering and to better understand the principles underneath.

The data resulting from our simulation is validated against the results of d'Eon [2] and agrees with them. The evaluation for our model will be comparing it to the ground truth, i.e. Monte-Carlo path tracing, by implementing our model in a well known rendering software, as Mitsuba for instance. We can also reproduce virtual scenes from real experiments to check the differences. Our ray tracer can be validated by the same procedure.

Our future objectives are to extend the analysis of our data to spatial dimensions, in order to complete the model. Then, we will search on how taking advantage of parallelism to speed up the underneath algorithms. We also want to study in greater depth the effects of single scattering, and how to integrate it efficiently in our model.

**Acknowledgments:** I would like to thank Nicolas HOLZSCHUCH for his explanations as well as his encouragement. I would also thank all people of the MAVERICK team in general for the great atmosphere that come out of this team. At last, I would thank INRIA for having accepted me for this project.



# Bibliography

- [1] E. d'Eon. A better dipole. <http://www.eugenedeon.com/papers/betterdipole.pdf>, 2012.
- [2] E. d'Eon and G. Irving. A quantized-diffusion model for rendering translucent materials. *ACM Transactions on Graphics (TOG)*, 30(4):56, 2011.
- [3] C. Donner, J. Lawrence, R. Ramamoorthi, T. Hachisuka, H. W. Jensen, and S. Nayar. An empirical bssrdf model. *ACM Transactions on Graphics (TOG)*, 28(3):30, 2009.
- [4] R. Green. Spherical harmonic lighting: The gritty details. In *Game Developers Conference*, 2003.
- [5] C. C. Grosjean. A high accuracy approximation for solving multiple scattering problems in infinite homogeneous media. *Il Nuovo Cimento*, 3(6):1262–1275, 1956.
- [6] H. W. Jensen, S. R. Marschner, M. Levoy, and P. Hanrahan. A practical model for subsurface light transport. In *Proceedings of the 28th annual conference on Computer graphics and interactive techniques*, pages 511–518. ACM, 2001.
- [7] S. Narasimhan, R. Ramamoorthi, and S. Nayar. Analytic rendering of multiple scattering in participating media. *ACM Transactions on Graphics (TOG)*, 2004.
- [8] S. G. Narasimhan, M. Gupta, C. Donner, R. Ramamoorthi, S. K. Nayar, and H. W. Jensen. Acquiring scattering properties of participating media by dilution. *ACM Transactions on Graphics (TOG)*, 25(3):1003–1012, 2006.
- [9] F. E. Nicodemus, J. C. Richmond, J. J. Hsia, I. W. Ginsberg, and T. Limperis. *Geometrical considerations and nomenclature for reflectance*, volume 160. US Department of Commerce, National Bureau of Standards, 1977.
- [10] E. Vitkin, V. Turzhitsky, L. Qiu, L. Guo, I. Itzkan, E. B. Hanlon, and L. T. Perelman. Photon diffusion near the point-of-entry in anisotropically scattering turbid media. *Nature communications*, 2:587, 2011.
- [11] J. Wang, P. Ren, M. Gong, J. Snyder, and B. Guo. All-frequency rendering of dynamic, spatially-varying reflectance. *ACM Transactions on Graphics (TOG)*, 28(5):133, 2009.